Quantum Effects on Vibrational and Electronic Spectra of Hydrazine Studied by "On-the-Fly" ab Initio Ring Polymer Molecular Dynamics†

Anna Kaczmarek,*,‡,§ Motoyuki Shiga,‡,|| and Dominik Marx‡

Lehrstuhl für Theoretische Chemie, Ruhr-Universität Bochum, 44780 Bochum, Germany, Faculty of Chemistry, Nicolaus Copernicus University, Gagarina 7, 87-100 Toruń, Poland, and Center for Computational Science and E-Systems, Japan Atomic Energy Agency, Higashi-Ueno 6-9-3, Taito-ku, Tokyo 110-0015, Japan

Received: September 15, 2008; Revised Manuscript Received: November 27, 2008

Structural and spectroscopic properties of hydrazine, H_2N-NH_2, it being a floppy or fluxional molecule in a vacuum, are investigated by means of ab initio molecular dynamics, ab initio path integral molecular dynamics, and ab initio ring polymer molecular dynamics simulations in conjunction with "on-the-fly" MP2 and CIS(D) electronic structure calculations. Whereas the former method relies on the classical approximation of nuclear motion, quantum effects on structure and dynamics are taken into account at finite temperatures by ab initio path integral and ab initio ring polymer molecular dynamics, respectively. It is shown that quantum-mechanical fluctuation effects of the nuclei, in addition to their purely thermal activation, cause significant configurational fluctuations due to strongly anharmonic vibrations and thus increase the explored regions on the Born−Oppenheimer potential energy surface at room temperature. Including these effects, in turn, leads to significant improvements in the computed spectra compared to stick spectra obtained at the equilibrium structure by means of harmonic normal-mode analysis, as well as by classical ab initio molecular dynamics. This family of methods, combining electronic structure with path integrals, offers a powerful and general computational approach not only to molecular structure determination of floppy or fluxional molecules, but also to evaluation of their electronic and vibrational spectra.

Introduction

Many molecules are known to exhibit large changes due to thermal vibrations in conjunction with quantum effects such as zero-point motion and tunneling. In the interesting limit of large-amplitude motion,[1,2] this results in what is often called "fluxional behavior" or "floppiness", which intertwines dynamics intimately with molecular structure and properties. The hydrazine molecule, H_2N-NH_2, is a particularly interesting case as it exhibits a twofold degenerate global minimum due to two enantiomers, **A** and **B**, in gauche conformation of C_2 symmetry,[3−8] as depicted in Figure 1. These two enantiomers can be interconverted by two qualitatively different mechanisms, via either by rotation of one $-NH_2$ moiety around the N−N bond or by inversion of one $-NH_2$ moiety at the nitrogen atom.[9] It has been reported that the energy barrier along the inversion pathway is slightly higher than that in the case of the ammonia molecule and the barrier for the internal rotation pathway via the anti-configuration is lower than that involving the syn configuration.[6] What still remains unexplored is the impact of fluctuations, both thermal and quantum mechanical, on intramolecular large-amplitude motion and thus on isomerization of the hydrazine molecule, which requires calculations beyond the static/harmonic approach.

Furthermore, it is known from experiment that hydrazine has a continuous ultraviolet (UV) spectrum with several broad peaks within a range of 120−240 nm according to ref 10. Static ab initio calculations based on both the self-consistent field (SCF) procedure[11] and multireference configuration interaction (MRCI) calculations[12] have shown that mostly Rydberg transitions are involved in this energy range. However, the information obtained from static calculations is limited since, in contrast to experiment, only a discrete spectrum can be obtained as the molecular structure is assumed to be frozen at the equilibrium structure. But in view of the large-amplitude motion discussed above, it is unclear to what extent such single-point approaches are valid. Therefore, it is essential to take into account molecular vibrations in the calculations to get insights into the continuous

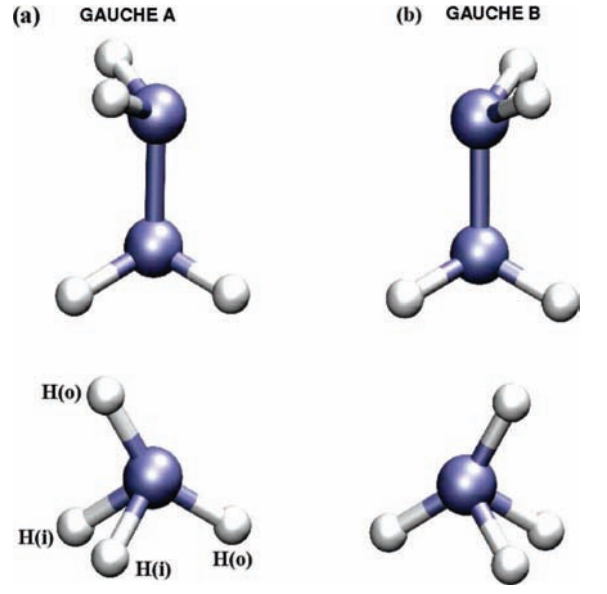

Figure 1. Hydrazine enantiomers: side and top views. Connecting transition states are depicted in Figure 2.

† Part of the "Max Wolfsberg Festschrift".

* To whom correspondence should be addressed. Fax: +48 (56) 654 24 77. E-mail: teoadk@chem.uni.torun.pl.

‡ Ruhr-Universität Bochum.

§ Nicolaus Copernicus University.

|| Japan Atomic Energy Agency.

10.1021/jp8081936 CCC: $40.75
Published on Web 01/22/2009

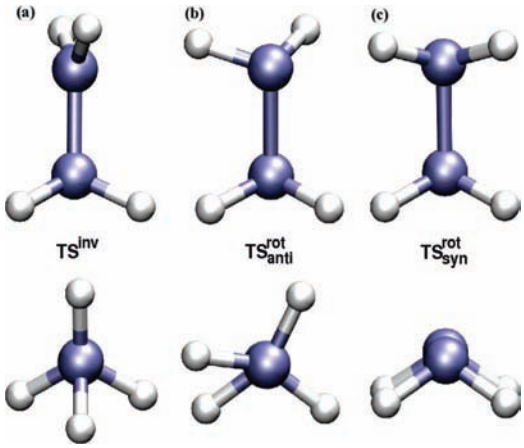

Figure 2. Transition states for the inversion and rotation mechanisms in hydrazine: side and top views.

and broad character of the electronic spectrum. In addition, in the energy range where the levels of the excited states appear, vibrational effects might also influence the spectral peak positions in the sense that a single peak may physically result from a confluence of different but overlapping resonances. One should note, moreover, that the peak positions obtained from the static calculations reported thus far for hydrazine do not agree satisfactorily with the experimental data (see Figure 1 in ref 12).

The vibrational spectrum of hydrazine is well studied by means of infrared (IR) absorption spectroscopy. Its IR spectrum consists of several intense signals below 1700 cm^{-1} and weaker resonances in the range of 3200−3300 cm^{-1} ascribed to N−H bond stretches.[8,13,14] Since the hydrazine molecule is floppy, one can expect significant anharmonicity in the intramolecular motion which might affect the IR spectrum. Indeed, evidence is provided by several reports that adding a posteriori anharmonic corrections on top of the ab initio normal-mode analysis improves the agreement with experimental data.[8,15] Still, this can only be a first step toward computing fully coupled anharmonic IR spectra in view of the large-amplitude character of the intramolecular motion within H_2N-NH_2.

Building upon Feynman's path integral formulation of quantum statistical mechanics[16−18] and its use in computer simulations[19−21] by implementing the ring polymer isomorphism,[22,23] the so-called ab initio path integral simulation techniques[24−28] have been very successful in elucidating the above-mentioned fluxional behavior of small molecules as well as hydrogen-bonded and metal clusters[24−43] (for reviews on these techniques see refs 44−46). Importantly, using the path integral formulation[16−18] of quantum statistical mechanics offers the unique possibility to switch on and off quantum effects on nuclei in *complex molecular systems at finite temperatures*, including liquids[47−49] and solids,[50−52] while staying within the identical methodological framework down to the level of using the same computer code. As a result, this trick allows one to separate, in a controlled and clean way, effects due to simple thermal activation from those more intricate fluctuation effects that are introduced due to nuclear quantum mechanics such as zero-point motion and tunneling. In addition, these full quantum simulation methods allow conceptually easy but still asymptotically exact access to isotope effects,[53] transcending the harmonic approximation but still staying within the realms of the Born−Oppenheimer approximation, since it suffices to substitute appropriate nuclear masses (e.g., D for H) when evaluating the path integral by simulation (i.e., D_2N-ND_2 instead of H_2N-NH_2 in the present case). In this spirit, the classical limit of nuclear motion yields the largest "isotope effect" possible when compared to the full quantum simulation where light isotopes are used (i.e., H_2N-NH_2 here). This opens the doorway to study isotope effects[53] on proton transfer, heavy-atom tunneling, or vibrational amplitudes including Debye−Waller factors in condensed matter. Similar access to kinetic isotope effects[53,54] is more tricky since it requires explicit generation of the quantum-mechanical time evolution of chemical reactions involving many coupled anharmonic degrees of freedom. Here, a step forward in this direction is reported by computing quantum effects on IR spectra along these lines but in the sense of a quasi-classical approximation, vide infra.

All calculations presented in this article employ the ab initio path integral molecular dynamics variant[24,25] using the Born−Oppenheimer propagation scheme[32,33] in conjunction with a "quantum chemical approach" to solve the electronic structure problem "on-the-fly" based on the MP2 method and atom-centered Gaussian basis sets. In particular, the hydrazine molecule, N_2H_4, is studied at room temperature to probe the effects of quantum and/or thermal fluctuations on structure and dynamics as well as on UV and IR spectra. To obtain IR and UV spectra directly from first principles, we have first of all performed standard ab initio molecular dynamics simulations for reference, using the same Born−Oppenheimer propagation scheme,[44,45] to assess anharmonicity and mode coupling effects in the limit of assuming a purely classical/thermal behavior of the nuclei. For further improvement of these spectra, nuclear quantum effects have been included using the ring polymer molecular dynamics (RPMD) technique[55−57] (see also refs 58−62), being a practical approximation to exact quantum dynamics, in conjunction with "on-the-fly" electronic structure calculations This combination constitutes a dynamical extension of ab initio path integral simulations,[26] quite similar to adiabatic ab initio centroid molecular dynamics,[28] to establish a quasi-classical approximation to molecular quantum dynamics; we note in passing that this is the first report of computing IR spectra using "on-the-fly" ab initio RPMD calculation. Finally, the methodology needed for computing electronic spectra based on ab initio path integral simulations is the one derived earlier in ref 40.

The IR and UV spectra obtained by such full quantum simulations are compared to those obtained from stick spectra based on static optimizations, classical ab initio simulations, and experimental data. All ground-state energies, gradients, and dipole moments have been generated "on-the-fly" along both the path integral and classical trajectories using the efficient RI-MP2 implementation[63] in Turbomole,[64] whereas electronic excitations based thereupon have been calculated using the CIS(D) method,[65] all using Gaussian basis sets. This particular combination of methods is a powerful and general tool that allows one to study various molecular spectra of vast classes of molecules, complexes, and clusters beyond the specific case present here.

Methods and Technical Details

Electronic Structure Calculations. To achieve a reasonable compromise between accuracy and computational expenses, the resolution-of-identity second-order Møller−Plesset perturbation theory (RI-MP2)[63] with split valence polarization SV(P) basis set[66] as implemented in the Turbomole program package[64] has been used "on-the-fly" to treat the electronic structure consistently in all dynamical simulations (i.e., ab initio MD, ab initio PIMD, and ab initio RPMD calculations). However, a series of static calculations has been performed

first to check the accuracy of the RI-MP2/SV(P) electronic structure for hydrazine. The influence of the application of the relatively small basis set has been determined on the basis of the comparison of important data such as optimized structure and harmonic frequencies to the larger basis set results obtained by using the aug-cc-pVTZ basis.[67] Moreover, the quality of the RI-MP2 approach for the specific system under investigation has been confirmed by comparing to plain MP2 results, to higher-level ab initio calculations, and to experimental data available in the literature.[8,13,14]

All calculations of UV spectra have been carried out using the configuration interaction approach, including single excitations and a perturbative correction for double excitations according to the CIS(D) method[65] as implemented in Gaussian03.[68] For these calculations, one has to take special care of the basis set to properly describe the Rydberg state excitations of hydrazine. Therefore, the split valence plus double Rydberg SV+DR basis set[69] has been employed for this purpose. Again, the quality of this particular electronic structure approach was assessed carefully by comparing static calculations using CIS(D)/SV+DR to those obtained with a larger 6−311++G(d,p) basis set as well as to higher-level ab initio results available from the literature.

Quantum and Classical ab Initio Simulations. The ab initio MD, ab initio PIMD, and ab initio RPMD simulations were carried out using the in-house Born−Oppenheimer molecular dynamics[44,45] code,[70] which is linked to the Turbomole program package.[64] The Born−Oppenheimer potential energy and the gradient based on RI-MP2/SV(P) are calculated "on-the-fly" during all these simulations using a time step of 0.2-fs duration. The massive Nosé−Hoover chain thermostat technique[71] is used to most efficiently equilibrate[71−73] the system and to establish the canonical ensemble at room temperatures, 300 K, and all path integrals have been Trotter-discretized using $P = 16$ beads according to ref 43. The ab initio PIMD simulations have been carried out for about 40 000 Born−Oppenheimer steps (corresponding formally to 8 ps), while the ab initio MD simulation (which corresponds to the $P = 1$ limit) has been continued for 100 ps (corresponding to 500 000 time steps). Energy conservation is satisfied within an error of about 0.0001 au for each trajectory.

Excited States: Computing UV Spectra. The methodology to compute electronic spectra based on ab initio path integral simulations, or using classical ab initio MD simulations as the consistent classical limit, has been worked out before[40] and applied to a small metal cluster. The method is based on first principles calculations, and it is in general applicable to many-body systems. It involves, however, an approximation suggested a long time ago by Lax,[74] which improves systematically with the increase of the nuclear mass and/or the decrease of the curvature of the involved potential energy surfaces.[40] Nevertheless, the quality of this method has not yet been assessed for truly molecular systems. From the methodological point of view, it is of particular interest to see how this method works for a floppy molecule such as hydrazine where accurate electronic spectra are known experimentally.

According to ref 40, the approximate photoabsorption cross section can be computed by collecting the vertical excitations of molecular configurations generated along ab initio trajectories using the relation

$$\sigma(\omega) \approx \left(\frac{2\pi^2 e^2}{m_e 4\pi\varepsilon_0 c}\right)\left\langle \sum_m f_{m0}\delta(\omega - \omega_{m,0})\right\rangle \qquad (1)$$

where $\langle ... \rangle$ is either the corresponding quantum statistical or thermal average. The first factor consists of physical constants such as the speed of light c, charge e and mass m_e of an electron, and the vacuum permittivity ε_0. The second factor is the statistical average of the oscillator strengths f_{m0} at frequencies $\omega = \omega_{m0}$, where $\hbar\omega_{m,0}$ is the excitation energy of the m-th electronic state. The f_{m0} and $\omega_{m,0}$ values are calculated at molecular configurations sampled along the canonical ab initio PIMD or MD trajectories generated using consistently RI-MP2/SV(P) energies and gradients.

To converge the UV spectrum of hydrazine in the gas phase, a total of 12 800 and 5000 structures were extracted from the ab initio PIMD and MD trajectories, respectively. One should repeat that RI-MP2/SV(P) electronic structure calculations have been used to generate the trajectories and thus the molecular configurations, whereas CIS(D)/SV+DR has been employed to compute f_{m0} and ω_{m0} and thus the UV spectra as explained in the Electronic Structure Calculations.

Quantum Dynamics: Computing IR Spectra. As is well-known, the IR absorption coefficient per unit volume can be written as[75]

$$\alpha(\omega) = \frac{4\pi^2\omega}{3\hbar c n(\omega)}\beta\hbar\omega I(\omega) \qquad (2)$$

where $\beta = 1/k_B T$, k_B is the Boltzmann constant, $n(\omega)$ is the refractive index assumed to be $n(\omega) = 1$ in the gas phase, and $I(\omega)$ is the Fourier transform of the Kubo-transformed dipole time-autocorrelation function $C_K(t)$:

$$I(\omega) = \frac{1}{2\pi}\int_{-\infty}^{\infty} dt\, \exp(-i\omega t) C_K(t) \qquad (3)$$

where

$$C_K(t) = \left\langle \frac{1}{\beta}\int_0^\beta d\lambda\, \hat{\mathbf{M}}(0)\hat{\mathbf{M}}(t + i\hbar\lambda)\right\rangle \qquad (4)$$

is the Kubo-transformed form of the autocorrelation function for the dipole moment operator $\hat{\mathbf{M}}$. Equation 2 is obtained by combining eqs 2 and 24 in ref 75 with the unit volume $V = 1$.

Next, in the RPMD approximation to quantum dynamics, molecular quantum configurations expressed in terms of a path integral, which is discretized using the lowest-order Trotter approximation for a given bead number P (see ref 46 for a review), are propagated in time by solving the RPMD equations of motion[55] (see also refs 58−62). They are obtained from standard PIMD by setting the fictitious masses equal to $1/P$ of the original nuclear mass[58] (note that in the normal mode representation of beads this is equivalent to setting all the fictitious masses of the modes equal to the original nuclear mass[76,77]). Then, the Kubo-transformed autocorrelation function is approximately obtained by calculating the dipole autocorrelation function from the RPMD trajectory as

$$C_K(t) \approx \langle \bar{\mathbf{M}}(0)\bar{\mathbf{M}}(t)\rangle_{rpmd} \qquad (5)$$

where $\bar{\mathbf{M}}(t) = 1/P\sum_{s=1}^{P} M_s(t)$ is the average over P beads. Note that there is no additional approximation needed to evaluate the autocorrelation functions of the nonlinear operator $\hat{\mathbf{M}}$ unlike in centroid molecular dynamics. Unlike in PIMD, thermostats must not be used in RPMD, and therefore, the thermal average in eq 5 must be taken among independent RPMD trajectories to get a converged result of the IR spectrum.

Finally, we mention that due to methodological intricacies RPMD can introduce artifacts[59,76] into computed vibrational or IR spectra because of resonance couplings between ring polymer and physical modes. This depends strongly on the specfic case and we refer to ref 77 for a detailed technical analysis of these artifacts that do not appear to be relevant here.

The setup for these "on-the-fly" ab initio RPMD simulations is closely analogous to that used for ab initio PIMD: $P = 16$ beads, temperature of $T = 300$ K, time step of 0.2 fs, and using RI-MP2/SV(P) electronic structure with the crucial exception of not thermostatting the RPMD runs. The initial conditions to launch independent ab initio RPMD runs to establish the canonical ensemble at 300 K on the level of the correlation functions according to eq 5 have been sampled from previously generated canonical ab initio PIMD trajectories that were massively thermostatted at $T = 300$ K using separate Nosé−Hoover chains[71−73] on each nuclear degree on freedom. The initial velocities for RPMD have been scaled properly such that the temperature of the system remains at 300 K. To generate the proper dynamics of an isolated molecule where only the internal ro-vibrational degrees of freedom are excited, the velocity components contributing to total translational and total rotational motions have been eliminated at every time step in RPMD.[77] In addition, the total linear and angular momenta have been reset to zero. For ab initio RPMD, 10 trajectories of a length of a 2 ps each (i.e., 10 000 time steps) were generated using this protocol; the final IR spectra reported were obtained as linear averages from the 10 individual spectra. Similarly, classical ab initio MD simulations were performed (using the $P = 1$ limit) in the same way except that the average is based on 20 microcanonical trajectories sampled from canonical trajectories generated again at $T = 300$.

Finally, it is stressed that these ab initio RPMD trajectories are also the basis to analyze the dynamics of hydrazine as a function of time within the framework of a quasi-classical approach. Similarly to computing the expectation value of the dipole operator as a function of time, any structural observable $\hat{O}$, such as distances, angles, or dihedrals, can be approximated by averaging over all P beads for each RPMD time step which yields the quasi-classical time evolution of the respective observable. One of the ways to define the expectation value of the observable $\hat{O}$ at time t under the condition that the initial structure is $R(0)$ is in terms of the Kubo-transformed form of time correlation functions:

$$\langle O(\mathbf{R}(0), t)\rangle \equiv \frac{\left\langle \frac{1}{\beta}\int_0^\beta \mathrm{d}\lambda\ \delta(\hat{\mathbf{R}} - \mathbf{R}(0))\hat{O}(t + i\hbar\lambda)\right\rangle}{\left\langle \frac{1}{\beta}\int_0^\beta \mathrm{d}\lambda\ \delta(\hat{\mathbf{R}} - \mathbf{R}(0))\right\rangle} \quad (6)$$

where the δ function stems from the structural constraint at $t = 0$. This is equivalent to the definition

$$\langle O(\mathbf{R}(0), t)\rangle \equiv \frac{\mathrm{Tr}\left[\hat{\rho}(\mathbf{R}(0))\exp\left(\frac{i\hat{H}t}{\hbar}\right)\hat{O}\exp\left(-\frac{i\hat{H}t}{\hbar}\right)\right]}{\mathrm{Tr}[\hat{\rho}(\mathbf{R}(0))]} \quad (7)$$

where the density operator $\hat{\rho}(\mathbf{R}(0))$, which determines the constraint, is assumed to have the symmetric form

$$\hat{\rho}(\mathbf{R}(0)) = \frac{1}{\beta}\int_0^\beta \mathrm{d}\lambda\ \exp(-(\beta - \lambda)\hat{H})\delta(\hat{\mathbf{R}} - \mathbf{R}(0))\exp(-\lambda\hat{H}) \quad (8)$$

in the sense of an *Ansatz* for the initial density matrix. In RPMD, the approximation of eq 6 is introduced as a conditional average

$$\langle O(\mathbf{R}(0), t)\rangle \approx \frac{\langle \bar{\delta}(0)\bar{O}(t)\rangle_{\mathrm{rpmd}}}{\langle \bar{\delta}(0)\rangle_{\mathrm{rpmd}}} \quad (9)$$

where $\bar{\delta}(0) = 1/P\sum_{s=1}^{P}\delta(\mathbf{R}_s - \mathbf{R}(0))$ and $\bar{O}(t) = 1/P\sum_{s=1}^{P}O(\mathbf{R}_s(t))$. Thus, eq 9 corresponds to the expectation value of the bead average of the observable along the RPMD trajectory starting from the initial set of bead configurations $(\mathbf{R}_1(0),..., \mathbf{R}_P(0))$ at $t = 0$. Therefore, this approximation allows one to extract insights into the quantum dynamics of a molecular system including mechanism and pathways of individual isomerization events subject to quantum effects on the nuclear dynamics. This information can be contrasted to the classical limit of nuclear time evolution where isomerization can only be driven by purely thermal activation.

TABLE 1: Structural Parameters of the Hydrazine Molecule[a]

basis set	SV(P)		aug-cc-pVTZ		cc-pCVTZ	
method	RI-MP2	MP2	RI-MP2	MP2	CCSD(T)[b]	expt[c]
Bond Length						
N−N	1.414	1.413	1.434	1.427	1.441	1.446
N−H(i)	1.023	1.023	1.014	1.011	1.014	1.016
N−H(o)	1.019	1.019	1.010	1.008	1.011	1.016
Valence Angle						
N−N−H(i)	113.0	113.0	111.7	112.0	110.9	108.85
N−N−H(o)	108.5	108.6	107.1	107.5	106.3	108.85
H(i)−N−H(o)	108.2	108.2	107.6	108.0	106.7	106
Dihedral Angle						
H(i)−N−N−H(o)	−89.8	−89.8	−89.9	−89.5	−89.6	−88.05

[a] Atom labelling according to Figure 1. All distances are given in angstroms and all angles in degrees. [b] Reference 8. [c] See ref 11 in ref 8.

Results and Discussion

Static Calculations: Equilibrium Structure and Harmonic Frequencies. This subsection presents the results of the static calculations performed not only to set up the ab initio MD, ab initio PIMD, and ab initio RPMD simulations, but also to compare the quality of the selected electronic structure treatments of ground and excited states to more sophisticated approaches. Structural parameters for hydrazine were calculated using the RI-MP2 and plain MP2 methods in conjunction with SV(P) and aug-cc-pVTZ basis sets; see the Electronic Structure Calculations for details. The data are summarized in Table 1 and compared to CCSD(T) data as well as to the experimental values (see ref 8 and literature cited therein). One can see that the RI-MP2 values are very close to MP2 values as expected and finds that the difference of small-size SV(P) and large-size aug-cc-pVTZ basis set data is not significant. Consequently, the RI-MP2/SV(P) values are in good agreement with both our MP2/aug-cc-pVTZ data and published CCSD(T) reference results within the error of ∼0.03 Å for bond lengths and about 3° for bond angles. Therefore, RI-MP2 with the modest SV(P) basis set is demonstrated to be an ideal electronic structure method for performing ab initio MD, ab initio PIMD, and ab initio RPMD simulations of hydrazine, which require tens of thousands of total energy and gradient computations per run according to the Methods and Technical Details, in view of its favorable compromise between accuracy and computational costs.

The same positive conclusion as to the performance of the RI-MP2/SV(P) approach for the specific molecule of interest can be drawn on the basis of the harmonic vibrational analysis data presented in Table 2. For RI-MP2/SV(P) frequencies, the average deviation from the CCSD(T) reference data from the literature[8] is the smallest from all investigated methods with that basis set and only about 5 cm^{-1} larger than with the more accurate RI-MP2/aug-cc-pVTZ method that is, however, much more demanding computationally. In addition,

TABLE 2: Unscaled Frequencies of the Hydrazine Molecule[a]

basis set	SV(P)		aug-cc-pVTZ		cc-pCVTZ				
method	RI-MP2	MP2	RI-MP2	MP2	CCSD(T)[b]	expt[c]	MD	RPMD	CC-VSCF[d]
torsion	489	485	435	444	404	377	466	469	457
NH_2 sym wagging	859	855	833	824	858	780	815	780	838
NH_2 asym wagging	1022	1022	1004	999	1045	966	999	966	989
N−N stretch	1184	1188	1132	1139	1130	875	1168	1151	1122
NH_2 twist	1338	1339	1307	1310	1316	933	1332	1302	1287
NH_2 twist	1376	1375	1341	1347	1350	1098	1368	1334	1318
NH_2 scissor	1722	1723	1675	1683	1679	1275	1700	1683	1647
NH_2 scissor	1735	1735	1687	1696	1693	1312	1735	1741	1666
NH_2 sym stretch	3458	3434	3508	3509	3471	3261	3418	3335	3309
NH_2 sym stretch	3460	3463	3510	3539	3482	3280	3469	3418	3335
NH_2 asym stretch	3582	3574	3620	3626	3577	3330	3568	3470	3445
NH_2 asym stretch	3586	3585	3623	3637	3582	3350	3578	3551	3430
average deviation	30	30	23	25	0				
maximum deviation	80	81	43	57	0				

[a] Note that harmonic values are reported for the static (RI-)MP2 and CCSD(T) calculations, whereas anharmonic values are obtained using ab initio MD and ab initio RPMD simulations (based on RI-MP2/SV(P) electronic structure), the CC-VSCF method, as well as in experiment. All frequencies are given in cm^{-1}. [b] Reference 8. [c] See ref 15 in ref 8. [d] Reference 15.

TABLE 3: Barriers to Internal Rotation around the N−N Bond and to Inversion on the Nitrogen Atom Relative to the Energy of the C_2 Ground-State Minima (See Figure 1 for Structure)[a]

	RI-MP2 SV(P)		MP2 SV(P)		RI-MP2 aug-cc-pVTZ		MP2 aug-cc-pVTZ		CCSD(T)[b] aug-cc-pVQZ	expt[c]
structure	ΔE	$\Delta(E + \mathrm{ZPE})$	ΔE	$\Delta(E + \mathrm{ZPE})$	ΔE	$\Delta(E + \mathrm{ZPE})$	ΔE	$\Delta(E + \mathrm{ZPE})$	ΔE	
TS_{syn}^{rot}	11.13	10.34	11.14	10.35	8.58	7.78	8.58	7.81	8.28	
TS_{anti}^{rot}	2.71	2.23	2.72	2.23	2.78	2.18	2.78	2.20	2.60	3.145
TS^{inv}	4.70	3.90	4.69	3.89	5.13	4.44	5.13	4.45	5.48	

[a] Here, TS_{syn}^{rot}, TS_{anti}^{rot}, and TS^{inv} denote the transition states corresponding to the rotation and inversion mechanism, respectively (see Figure 2 for structures). The zero-point energy (ZPE) corrections are evaluated using the unscaled harmonic frequencies reported in Table 2. All energies are given in kilocalories per mole. [b] For the geometry optimized at the MP2/aug-cc-pVQZ level of theory. [c] Reference 5.

the maximal error of the RI-MP2/SV(P) results is observed for the rather unimportant lowest frequency mode, which nevertheless strongly influences the average error of the method.

As explained in the Introduction, the hydrazine molecule can exist in two enantiomeric forms. This fact is not crucial for the present study since most of the chemical properties such as UV and IR spectra among others do not depend on the chirality of the system. However, the calculated barrier height for the interconversion between the two enantiomers (i.e., the isomerization barrier or transition-state energy) will yield another benchmark for the quality of the electronic structure method employed in the present study. The comparison of these data collected in Table 3 with the estimates of the barrier heights from the literature shows that acceptable agreement is achieved with the economical RI-MP2/SV(P) approach. The rotation around the N−N bond proceeding via the TS_{anti}^{rot} transition state is characterized by the lowest barrier of less than about 3 kcal/mol, while the highest barrier is expected for the transition via TS_{syn}^{rot}; following IUPAC nomenclature,[78] "anti" denotes the form characterized by the values of the torsional angle between the nitrogen lone pairs in the range from ±90 to 180°, whereas "syn" corresponds to the respective values from 0 to ±90° (Figure 2). These data are confirmed by the calculations performed with significantly larger basis sets using in addition the plain MP2 method. The ordering of the barrier height remains the same for all analyzed methods, and most importantly, it is consistent with both high-level ab initio calculations and experimental findings.[5,6,9] These results provide additional justification for the choice of the RI-MP2/SV(P) method for the "on-the-fly" classical and quantum dynamics to be discussed in the next section.

Dynamic Simulations: Fluctuation Effects on Structure. The time-averaged statistical analysis of the ab initio MD and ab initio PIMD simulations is presented in this subsection, where the quantum canonical ensemble is sampled on the basis of the generated configurations. Panels (a) and (b) of Figure 1 represent the two enantiomers of different chirality. Although the enantiomers should be found with the same statistical probability, in practice it is difficult to reproduce this fact because the generic simulation time scale is not long enough to equally sample two structures that are separated by a high potential barrier. Thus, only the properties that are independent of chirality are discussed in the present contribution.

Figures 3, 4, and 5 show normalized distribution functions for bond lengths, bond angles, and dihedral angles, respectively, obtained from ab initio MD ("classical") and ab initio PIMD ("quantum") simulations together with the data corresponding to the equilibrium structure marked by vertical lines. It should be noted that for the dihedral angle ϕ the distribution is presented as a function of its absolute value $|\phi|$ to symmetrize it with respect to the chiral symmetry; note that such symmetrization could be avoided by sampling more extensively the underlying isomerization events, which however would amount to a significant increase of computer time in view of the barrier heights involved, or to using accelerated ab initio MD at the expense of destroying the Newtonian time evolution needed to compute the anharmonic IR spectrum in Dynamic Simulations: IR Spectra.

First of all, very large deviations from the static equilibrium values are observed for all these structural observables due to fluctuations at 300 K. Second, although qualitatively similar, significant differences between the classical and quantum results show that even at room temperature nuclear quantum effects

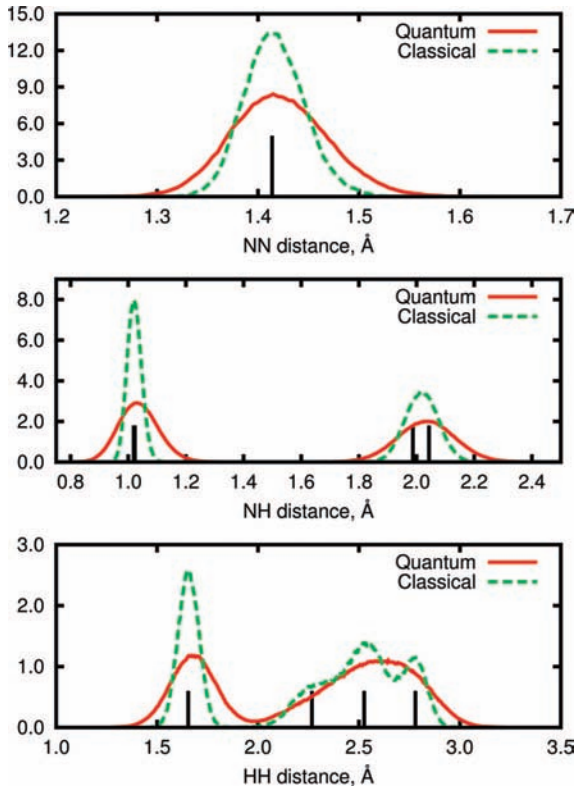

Figure 3. Bond length distributions from ab initio MD and ab initio PIMD simulations: upper panel corresponds to NN bond, middle panel to NH distances, and lower panel to HH distances. Vertical solid lines indicate equilibrium distances obtained from structure optimization.

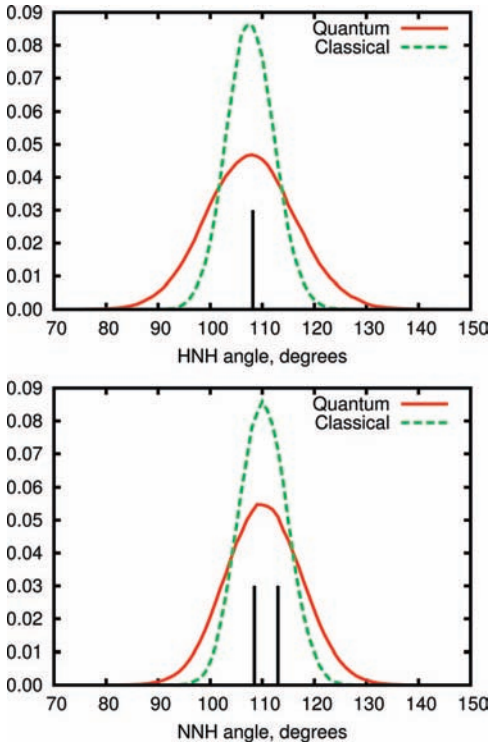

Figure 4. Bond angle distributions from ab initio MD and ab initio PIMD simulations: upper panel corresponds to HNH angles and lower panel depicts NNH angles. Vertical solid lines indicate equilibrium angles obtained from structure optimization.

cannot be neglected when it comes to a quantitative assessment as they contribute non-negligible additional broadening. In Figure 3, the first H−H peak is ascribed to the two hydrogen

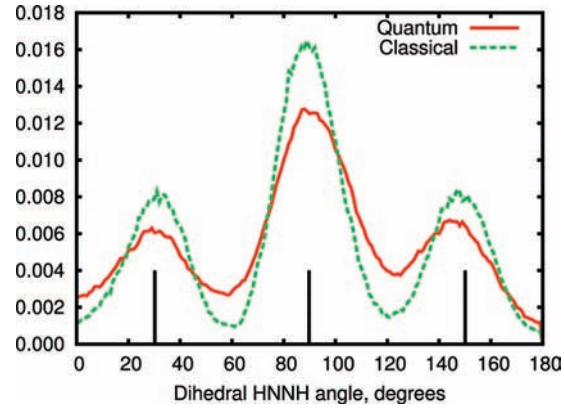

Figure 5. Absolute HNNH dihedral angle distribution from ab initio MD and ab initio PIMD simulations. Vertical solid lines indicate equilibrium angles obtained from structure optimization.

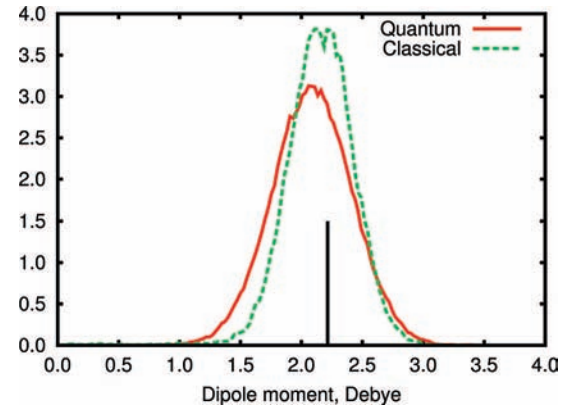

Figure 6. Dipole moment distribution from ab initio MD and ab initio PIMD simulations. Vertical solid line indicates equilibrium dipole moment obtained from structure optimization.

atoms bonded to the same nitrogen atom while the second group of the H−H peaks comes from two hydrogen atoms bonded to different nitrogen atoms. The classical ab initio MD simulation yields three well-pronounced maxima corresponding, respectively, to H(i)−H(i) (at about 2.25 Å), H(i)−H(o) (at ∼2.5 Å), and H(o)−H(o) (around 2.8 Å) distances with maxima close to the equilibrium values; see the definitions of H(i) and H(o) atoms in Figure 1. In contrast, these contributions are smeared out into one peak in the quantum ab initio PIMD simulation, which has its maximum at a distance where neither the equilibrium nor the classical distribution feature any peak! Thus, apart from dramatic broadening effects, large fluctuations induced by the quantum effects tend to enhance the vibrational anharmonicity, thereby increasing bond lengths systematically. For instance, the average N−H bond length from ab initio PIMD (∼1.04 Å) is slightly longer than that obtained from either ab initio MD (∼1.02 Å) or at equilibrium (∼1.02 Å) using all the identical RI-MP2/SV(P) electronic structure treatments. The quantum broadening is observed not only for the H−H and N−H distances where the light hydrogen atom is involved, but also for the N−N distances as demonstrated by the top panel of Figure 3. Likewise, Figures 4 and 5 show that the valence angle and dihedral angle distributions are strongly influenced as well by quantum-mechanical fluctuation effects on top of thermal broadening due to classical activation.

In Figure 6, the distribution of the total dipole moment (operator) from ab initio MD and ab initio PIMD calculations is shown; note that in both cases the dipole moment (operator) is evaluated consistently using the RI-MP2/SV(P) method along

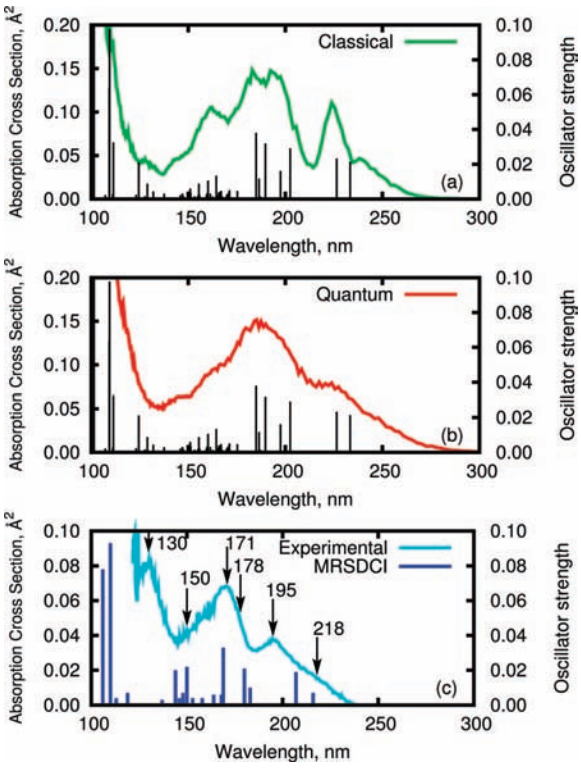

Figure 7. UV spectra for hydrazine molecule obtained from (a) "classical" ab initio MD simulation (solid line) using CIS(D)/SV+DR electronic structure for excitation energies (stick spectrum shown at equilibrium structure), (b) "quantum" ab initio PIMD simulation (solid line) using CIS(D)/SV+DR electronic structure for excitation energies (stick spectrum shown at equilibrium structure), and (c) static MRSDCI/(6−31G* +midbond functions) calculation (stick spectrum, taken from ref 12) and experiment (solid line, taken from ref 10). See text for details.

the generated trajectories. Again, fluctuations allow for strong excursions of the dipole moment away from its equilibrium value marked by the vertical line, thus leading to substantially broad distribution functions. Furthermore, it is noteworthy to observe that because of anhamonic coupled vibrations the average dipole moment (i.e., the expectation value of the dipole moment operator when using the ab initio PIMD full quantum method) is affected in addition. It is seen to decrease slightly in ab initio MD (∼2.16 D) and even more so after including quantum effects in ab initio PIMD (∼2.10 D) with respect to the static equilibrium value of ∼2.22 D; note that the experimental value is 1.85 D according to ref 79.

Dynamic Simulations: UV and Ionization Spectra. On the basis of the classical and quantum canonical simulations using ab initio MD and ab initio PIMD, the UV spectra obtained by using CIS(D)/SV+DR excitation energies are presented in Figure 7 and compared to both static multireference MRSDCI/(6−31G* + midbond functions) calculations[12] and experimental data.[10] In the limit of the stick spectrum obtained at the equilibrium structure, which serves as our internal static reference, it can be seen that the present CIS(D) results (see panel (a) or (b)) are acceptably close to the much more elaborate MRCI results[12] depicted in panel (c), although the agreement certainly cannot be perfect; the numbers are collected in Table 4. Thus, the CIS(D) stick spectrum can be grouped into four separate regions following the discussion as in the case of the MRCI calculation.[12] In the CIS(D) spectrum, regions I−III in the range from 140 nm to longer wavelengths correspond undoubtedly to the Rydberg transitions, while in region IV under

TABLE 4: UV Stick Spectra Obtained from Static Calculations at the Equilibrium Structure[a]

	6−311++G(d,p)		SV+DR		MRCI	expt
	CIS	CIS(D)	CIS	CIS(D)	ref 12	ref 10
S_1	173 (0.0222)	216	176 (0.0214)	233	216 (0.007)	218
S_2	170 (0.0253)	210	173 (0.0233)	226	207 (0.019)	195
S_3	150 (0.0346)	186	152 (0.0291)	202	183 (0.010)	178
S_4	148 (0.0143)	181	150 (0.0161)	198	180 (0.021)	171
S_5	144 (0.0070)	174	146 (0.0319)	190	169 (0.033)	150
S_6	144 (0.0197)	173	145 (0.0014)	187	168 (0.004)	130
S_7	137 (0.0109)	167	142 (0.0117)	186	168 (0.006)	
S_8	136 (0.0822)	167	141 (0.0380)	185	164 (0.006)	
S_9	115 (0.0535)	133	133 (0.0047)	174	158 (0.004)	
S_{10}	115 (0.0045)	131	131 (0.0041)	171	154 (0.001)	

[a] All excitation wavelengths are given in nanometers, and the corresponding oscillator strengths are reported in parentheses where available.

140 nm the valence transitions and higher Rydberg transitions are observed. However, because of the complex nature of the transitions involving the Rydberg states in conjunction with ambiguous classification methods it is not trivial to ascribe the respective signals to the actual molecular orbitals involved.

The experimental spectrum[10] of hydrazine is seen to exhibit three broad peaks at 195, 171, and 130 nm and additionally three more weak shoulders at 218, 178, and 155 nm (solid line in Figure 7c). The overall structure of the ab initio PIMD quantum spectra calculated using CIS(D)/SV+DR electronic structure corresponds surprisingly well to the experimental spectrum. It should be stressed that no artificial ("adjusted") broadening, for instance by using Gaussian or Lorentzian smearing, is necessary within the present approach since the trajectories properly generated in the canonical ensemble by thermostatting embody fluctuations and thus smearing effects (excluding electronic lifetime broadening) at constant temperature.[40] First, a hardly visible signal arising at 255 nm and the following peak at 225 nm in ab initio PIMD correlate well with the 218-nm shoulder on the long wavelength tail and with the corresponding band peak at 195 nm, respectively, found in the experiment. Comparing with the static calculation, one can see that these two signals are related to the first two states in the aforementioned region I. Next, the band at about 190−180 nm in ab initio PIMD, which is associated with region II states, corresponds to two peaks in the experimental spectrum appearing at 178 and 171 nm, respectively. The barely distinguished signal at 155 nm in ab initio PIMD, which is related to region III states, matches the weak shoulder present at 160 nm in experiment. The small peak on the high energy shoulder of the ab initio PIMD spectrum related to region IV states can be compared to the 130-nm band in the experimental spectrum. Unfortunately, the detailed assignment of the bands is currently not feasible particularly for higher energies because of the presence of a large number of states characterized by rather small oscillator strengths. Finally, the classical spectrum obtained from ab initio MD depicted in Figure 7a features sharp peaks and is too structured in general. This demonstrates nicely that it is advisable to include quantum effects on nuclear motion to appropriately smear out the sharp vertical excitation resonances due to ro-vibrational motion. Further to the conclusions drawn in Static Calculations: Equilibrium Structure and Harmonic Frequencies based on analysis of structure and dipole moment, this observation supports the concept that quantum-mechanical fluctuation effects on nuclear motion are "visible" even in UV spectra at room temperature.

Single-photon nonresonant ionization spectra can be approximately computed in a manner similar to that of UV spectra

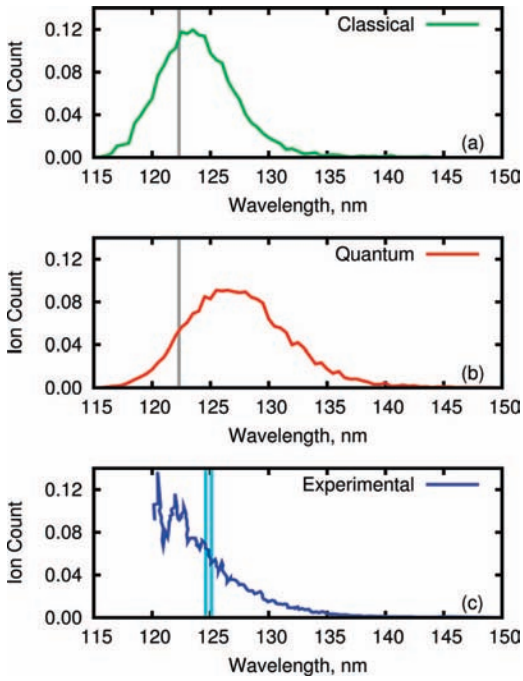

Figure 8. Single-photon ionization efficiency curves obtained from (a) "classical" ab initio MD simulation using MP2/6−311++G(d,p) electronic structure for ionization energies, (b) "quantum" ab initio PIMD simulation using MP2/6−311++G(d,p) electronic structure for ionization energies, and (c) experimental single-photon ionization efficiency curve (taken from ref 10). Vertical solid black lines in (a) and (b) indicate the MP2/6−311++G(d,p) vertical ionization energy at the equilibrium structure obtained from structure optimization (using RI-MP2/SV(P)), while the vertical solid light blue lines in (c) indicate the two different experimental vertical first ionization potentials (taken from ref 10).

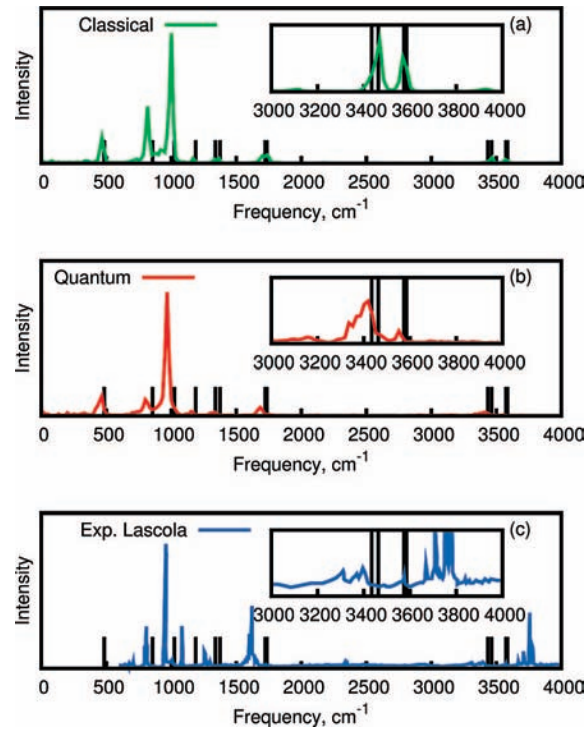

Figure 9. IR spectrum for hydrazine molecule from (a) "classical" ab initio MD simulation (solid line), (b) "quantum" ab initio RPMD simulation (solid line), and (c) experiments (solid line, taken from ref 13; the signals at 3600−3800 cm^{-1} come from the H_2O impurities absorption). Vertical solid lines indicate the corresponding harmonic stick spectra (without intensities) at the equilibrium structure obtained from structure optimization using the same RI-MP2/SV(P) electronic structure method.

by collecting ionization energy data computed for numerous configurations sampled from ab initio MD or ab initio PIMD trajectories. This is formally obtained if one neglects the dependence of the oscillator strength on nuclear coordinates in eq 1 between the ground and ionic states. Using this approach, we generated the photoionization spectrum of hydrazine presented in Figure 8 on the basis of MP2/6−311++G(d,p) ionization energies using a sample of configurations obtained from the thermostatted trajectories based on RI-MP2/SV(P) energies and gradients. Here, a basis set of triple-ζ quality was chosen to ensure an acceptable accuracy of the ionization energy of hydrazine. At the equilibrium structure the vertical ionization energy is 122.3 nm for MP2/6−311++G(d,p), which compares favorably to 122.1 nm calculated using the more accurate CASPT2 method.[12] Moreover, the experimental vertical ionization energy has been published to be about 124.6 or 125.1 nm according to ref 10. On the basis of these comparisons, the MP2/6−311++G(d,p) method is shown to be a reasonable choice of the computational methodology for the present dynamical simulations that require in total more than 25 000 single-point calculations of ionization energies to generate the broadened spectra depicted in Figure 8.

The classical and quantum ionization spectra are compared to the count data from single-photon ionization experiments[10] in Figure 8c. Although the ab initio PIMD quantum spectrum in panel (b) is red-shifted compared to the experimental one, the slope on the low-frequency wing of the computed spectrum is in fair agreement with experiment, in particular in view of the systematic offset from the experimental ionization potential(s) as indicated in (c) by the vertical lines. This pronounced wing can be traced back to *large-amplitude vibrations* in the electronic ground state of the floppy hydrazine molecule that enhance the sampling of those structural distortions of the molecular skeleton where ionization requires significantly less energy compared to the equilibrium structure. This most interesting phenomenon is clearly visible in the pronounced shift of the average ionization energy away from its equilibrium value when quantum-motion of the nuclear is included in Figure 8b, whereas not much of such a shift is visible in the limit of classical motion in panel (a) where the underlying electronic structure method is identical.

Dynamic Simulations: IR Spectra. The IR spectra of hydrazine at 300 K in the gas phase are depicted in Figure 9 again for the classical and quantum simulations using the RI-MP2/SV(P) method consistently to compute energies, gradients, and dipole moments. Note that here the "on-the-fly" ab initio RPMD method has been used instead of just ab initio PIMD to generate a physical time evolution of the dipole operator in the sense of a quasi-classical approximation to full quantum dynamics. For easier analysis of the presented data, the corresponding peak positions are listed in Table 2 together with the correlation-corrected vibrational self-consistent field (CC-VSCF) anharmonic data from ref 15, the static harmonic results, and the experimental positions. The signal of largest intensity which arises from NH_2 asymmetric wagging motion is found at 966 cm^{-1} and thus overlaps nicely with the experimental peak. Inclusion of the anharmonicity effects (i.e., passing from harmonic calculations obtained in the static limit to the classical ab initio MD simulation) causes a red-shift of most of the frequencies from several wavenumbers up to about 40 cm^{-1}.

Further quantitative improvement with respect to the experimental data is obtained after taking into account, in addition to

thermal fluctuations, the nuclear quantum effects which shift vibrational frequencies to the red by up to 50 cm^{-1} in addition. Comparison of these data to the experimental spectra[13,14] reveals the very good quality of these ab initio RPMD RI-MP2/SD(V) results. Although the N−H stretch modes are not in such a good agreement with experiment as other modes, ab initio RPMD gives significantly better results than ab initio MD and, of course, the standard normal-mode approximation. In addition, the "on-the-fly" RPMD spectrum corresponds well to the published VSCF anharmonic frequencies.[15] The discussion of vibrational spectroscopy by means of ab initio RPMD is closed by stressing that the quality of the calculation could obviously be improved upon, within the limitations of the RPMD approximation to quantum dynamics, when using a better electronic structure method in view of the differences between the MP2 and CCSD(T) data in the *harmonic* approximation according to the results compiled in Table 2. Although this is clearly not a limitation of our approach as such, dynamical calculations that improve systematically MP2 such as CCSD(T) are currently out of reach to be carried out in the framework of "on-the-fly" ab initio path integral simulations, such as RPMD, because of the required computer time needed even for such a rather small molecule as hydrazine.

Summary, Conclusions, and Outlook

In this contribution, structural and electronic properties of the hydrazine molecule, it being prone to large-amplitude motion, have been studied by a series of classical and quantum ab initio simulations at room temperature. In particular, ab initio molecular dynamics, ab initio path integral molecular dynamics, and ab initio ring polymer molecular dynamics simulations have been carried out using the MP2 method "on-the-fly" to access thermal and quantum fluctuation effects on molecular properties at finite temperatures, which can be compared to static calculations on the basis of the equilibrium structure. In addition to structure, the respective broadening effects on UV, ionization, and IR spectra have been decomposed in comparison to both stick spectra obtained using the same electronic structure method as well as experimental results.

It has been shown that using ab initio PIMD simulations, thus taking proper account of skeletal vibrations at finite temperatures due to both thermal and quantum effects, it is possible to reproduce the overall shape of the continuous UV spectrum. Classical dynamics, in contrast, yields a UV spectrum that is overstructured compared to that of experiment, characterized by a few structureless peaks on a broad background. When it comes to the stick spectrum obtained at the static equilibrium structure, unphysical a posteriori broadening procedures seem to be required to reproduce experiment. In addition, nuclear quantum effects offer a natural explanation of the pronounced tail of the single-photon ionization efficiency that is observed to extend to energies much lower than the vertical ionization energy at the equilibrium structure. Again, such quantum-mechanical fluctuation effects are shown to considerably improve the result obtained with classical ab initio MD, whereas the respective "stick spectrum" obtained at equilibrium cannot explain the phenomenon at all by definition. Moreover, ab initio RPMD simulations, providing a sort of quasi-classical approximation to quantum dynamics, were proven to be useful to compute the fully coupled anharmonic IR spectra from the Fourier transform of dipole autocorrelation functions in the room temperature regime. Thus, "...something is to be learned by 'observing' the motion of different isotopic species on the same potential surface."[53] considering classical nuclei as "infinitely heavy isotopes", vide ante.

Along these lines, it would be most interesting to probe quantum effects on the kinetics[54] and possibly on the mechanism of the intramolecular isomerization reaction that interconverts the two enantiomeric forms in view of internal soft modes along either rotation or inversion pathways, using hydrazine and perdeuterated hydrazine. Although this requires neither further methodological development nor additional implementations beyond ab initio RPMD, it would call for a considerable investment of computer time to sample these rare events without accelerating artificially (and thus destroying) the physical time evolution. Such simulations are particularly demanding in view of the need to generate long trajectories in conjunction with the requirement to sample many initial conditions because of the conditional averaging that must be carried out according to eq 9 to extract statistically meaningful conclusions.

Drawn from the above-mentioned results obtained for hydrazine, we believe that the methodology presented in this article establishes a powerful and general approach, based on ab initio path integrals, not only to molecular structure, in particular of floppy or fluxional molecules, but also to their electronic and vibrational spectra, including isotope effects. Obviously, there are still various quantitative discrepancies observed when comparing the spectra obtained from ab initio PIMD and ab initio RPMD to experimental data. This is, however, largely related to the limited accuracy of the underlying electronic structure methods (i.e., MP2 and CIS(D) calculations with small basis sets used in the present case), whereas methods such as CCSD(T) with large bases are known from a wealth of static calculations to be required to achieve predictive quality. Although not possible at the moment, we share the optimism that it will become feasible in the future to carry out such ab initio path integral simulations with "chemical accuracy" in view of advances of both parallel algorithms for correlated electronic structure calculations and computer technology.

Acknowledgment. We are indebted to Professors V. Staemmler and A. J. Sadlej for stimulating discussions on ultraviolet spectra and to Drs. H. Forbert, S. Ivanov, as well as to A. Witt for sharing with us their insights into quasi-classical quantum dynamics. Partial financial support of A.K. by DFG Forschergruppe FOR 618 on "Aggreation of Small Molecules" and of M.S. by a Humboldt Fellowship granted by the Alexander von Humboldt Foundation is gratefully acknowledged as well as general support of D.M. by FOR 618 and Fonds der Chemischen Industrie (FCI). Cyfronet Kraków is gratefully acknowledged for the allotment of the computational facilities as well as Bovilab@RUB and Rechnerverbund-NRW.

References and Notes

(1) Saykally, R. J. *Science* **1998**, *239*, 157.
(2) *Structure and Conformations of Non-Rigid Molecules*; Laane, J., Dakkouri, M., van der Veken, B., Oberhammer, H., Eds.; Kluwer: Dordrecht, The Netherlands, 1993.
(3) Kohata, K.; Fukuyama, T.; Kuchitsu, K. *J. Phys. Chem. A* **1982**, *86*, 602.
(4) Cabaleiro-Lago, E. M.; Ríos, M. A. *J. Phys. Chem. A* **1999**, *103*, 6468.
(5) Chung-Phillips, A.; Jebber, K. A. *J. Chem. Phys.* **1995**, *102*, 7080.
(6) Cowley, A.; Mitchell, D. J.; Whangbo, M.-H.; Wolfe, S. *J. Am. Chem. Soc.* **1979**, *101*, 5224.
(7) Schlegel, H. B.; Skancke, A. *J. Am. Chem. Soc.* **1993**, *115*, 7465.
(8) Machado, F. B. C.; Roberto-Neto, O. *Chem. Phys. Lett.* **2002**, *352*, 120.
(9) Dyczmons, V. *J. Phys. Chem. A* **2000**, *104*, 8263.
(10) Syage, J. A.; Cohen, R. B.; Steadman, J. *J. Chem. Phys.* **1992**, *97*, 6072.
(11) Staemmler, V. *Acta Phys. Pol., A* **1988**, *74*, 331.
(12) Habas, M.-P.; Baraille, I.; Larrieu, C.; Chaillet, M. *Chem. Phys.* **1997**, *219*, 63.

(13) Lascola, R.; Withnall, R.; Andrews, L. *Inorg. Chem.* **1988**, *27*, 642.
(14) Catalano, E.; Sanborn, R. H.; Frazer, J. W. *J. Chem. Phys.* **1963**, *38*, 2265.
(15) Kowal, A. T. *J. Mol. Struct.: THEOCHEM* **2003**, *625*, 71.
(16) Feynman, R. P.; Hibbs, A. R. *Quantum Mechanics and Path Integrals*; McGraw-Hill: New York, 1965.
(17) Feynman, R. P. *Statistical Mechanics; A Set of Lectures*; W. A. Benjamin: Reading, MA, 1972.
(18) Kleinert, H. *Path Integrals in Quantum Mechanics, Statistics, Polymer Physics, and Financial Markets*; World Scientific: Singapore, 2004.
(19) Fosdick, L. D. *J. Math. Phys.* **1962**, *3*, 1251.
(20) Fosdick, L. D.; Jordan, H. F. *Phys. Rev.* **1966**, *143*, 58.
(21) Jordan, H. F.; Fosdick, L. D. *Phys. Rev.* **1968**, *171*, 128.
(22) Chandler, D.; Wolynes, P. G. *J. Chem. Phys.* **1981**, *74*, 4078–4095.
(23) Ceperley, D. M. *Rev. Mod. Phys.* **1995**, *67*, 279.
(24) Shiga, M.; Tachikawa, M.; Miura, S. *Chem. Phys. Lett.* **2000**, *332*, 396.
(25) Shiga, M.; Tachikawa, M.; Miura, S. *J. Chem. Phys.* **2001**, *115*, 9149.
(26) Marx, D.; Parrinello, M. *Z. Phys. B: Condens. Matter* **1994**, *95*, 143.
(27) Marx, D.; Parrinello, M. *J. Chem. Phys.* **1996**, *104*, 4077.
(28) Marx, D.; Tuckerman, M. E.; Martyna, G. J. *Comput. Phys. Commun.* **1999**, *118*, 166.
(29) Marx, D.; Parrinello, M. *Nature (London)* **1995**, *375*, 216.
(30) Marx, D.; Parrinello, M. *Science* **1996**, *271*, 179.
(31) Tuckerman, M. E.; Marx, D.; Klein, M. L.; Parrinello, M. *Science* **1997**, *275*, 817.
(32) Štich, I.; Marx, D.; Parrinello, M.; Terakura, K. *Phys. Rev. Lett.* **1997**, *78*, 3669.
(33) Štich, I.; Marx, D.; Parrinello, M.; Terakura, K. *J. Chem. Phys.* **1997**, *107*, 9482.
(34) Rousseau, R.; Marx, D. *J. Chem. Phys.* **1999**, *111*, 5091.
(35) Kramer, G. M.; Oka, T.; White, E. T.; Marx, D.; Parrinello, M. *Science* **1999**, *286*, 1051.
(36) Tuckerman, M. E.; Marx, D. *Phys. Rev. Lett.* **2001**, *86*, 4946.
(37) Knoll, L.; Vager, Z.; Marx, D. *Phys. Rev. A* **2003**, *67*, 022506.
(38) Shiga, M.; Tachikawa, M. *Chem. Phys. Lett.* **2003**, *374*, 229.
(39) Tachikawa, M.; Shiga, M. *J. Chem. Phys.* **2004**, *121*, 5985.
(40) Sala, F. D.; Rousseau, R.; Görling, A.; Marx, D. *Phys. Rev. Lett.* **2004**, *92*, 183401.
(41) Tachikawa, M.; Shiga, M. *J. Am. Chem. Soc.* **2005**, *127*, 11908.
(42) Hayashi, A.; Shiga, M.; Tachikawa, M. *J. Chem. Phys.* **2006**, *125*, 204310.
(43) Ishibashi, H.; Hayashi, A.; Shiga, M.; Tachikawa, M. *ChemPhysChem* **2008**, *9*, 383.
(44) Marx, D.; Hutter, J. *Ab Initio Molecular Dynamics: Basic Theory and Advanced Methods*; Cambridge University Press: Cambridge, 2009.
(45) Marx, D.; Hutter, J. In *Modern Methods and Algorithms of Quantum Chemistry*; Grotendorst, J., Ed.; John von Neumann Institute for Computing, Forschungzentrum Jülich: Jülich, Germany, 2000; Vol. 1, pp 301−449. See http://www.theochem.rub.de/go/cprev.html for downloads.
(46) Tuckerman, M. E. In *Quantum Simulations of Complex Many-Body Systems: From Theory to Algorithms*; Grotendorst, J., Marx, D., Muramatsu, A., Eds.; John von Neumann Institute for Computing, Forschungzentrum Jülich: Jülich, Germany, 2002; Vol. 10.
(47) Marx, D.; Tuckerman, M. E.; Hutter, J.; Parrinello, M. *Nature (London)* **1999**, *397*, 601.
(48) Marx, D.; Tuckerman, M. E.; Parrinello, M. *J. Phys.: Condens. Matter* **2000**, *12*, A153.
(49) Tuckerman, M. E.; Marx, D.; Parrinello, M. *Nature (London)* **2002**, *417*, 925.
(50) Benoit, M.; Marx, D.; Parrinello, M. *Nature (London)* **1998**, *392*, 258.
(51) Biermann, S.; Hohl, D.; Marx, D. *Solid State Commun.* **1998**, *108*, 337.
(52) Benoit, M.; Marx, D. *ChemPhysChem* **2005**, *6*, 1738.
(53) Wolfsberg, M. *Annu. Rev. Phys. Chem.* **1969**, *20*, 449.
(54) Bigeleisen, J.; Wolfsberg, M. *Adv. Chem. Phys.* **1958**, *1*, 15.
(55) Craig, I. R.; Manolopoulos, D. E. *J. Chem. Phys.* **2004**, *121*, 3368.
(56) Miller, T. F.; Manolopoulos, D. E. *J. Chem. Phys.* **2005**, *123*, 154504.
(57) Braams, B. J.; Manolopoulos, D. E. *J. Chem. Phys.* **2006**, *125*, 124105.
(58) Hone, T. D.; Rossky, P. J.; Voth, G. A. *J. Chem. Phys.* **2006**, *124*, 154103.
(59) Habershon, S.; Fanourgakis, G. S.; Manolopoulos, D. E. *J. Chem. Phys.* **2008**, *129*, 074501.
(60) Yoshimori, A. *J. Chem. Phys.* **2008**, *128*, 234105.
(61) Hone, T. D.; Poulsen, J. A.; Rossky, P. J.; Manolopoulos, D. E. *J. Phys. Chem. B* **2008**, *112*, 294.
(62) Habershon, S.; Braams, B. J.; Manolopoulos, D. E. *J. Chem. Phys.* **2007**, *127*, 174108.
(63) Weigend, F.; Häser, M. *Theor. Chem. Acc.* **1997**, *97*, 331.
(64) Ahlrichs, R.; Bär, M.; Häser, M.; Horn, H.; Kölmel, C. *Chem. Phys. Lett.* **1989**, *162*, 165.
(65) Head-Gordon, M.; Rico, R. J.; Oumi, M.; Lee, T. J. *Chem. Phys. Lett.* **1994**, *219*, 21.
(66) Weigend, F.; Häser, M.; Patzelt, H.; Ahlrichs, R. *Chem. Phys. Lett.* **1998**, *294*, 143.
(67) Dunning, T. H. *J. Chem. Phys.* **1989**, *90*, 1007.
(68) Frisch, M. J.; Trucks, G. W.; Schlegel, H. B.; Scuseria, G. E.; Robb, M. A.; Cheeseman, J. R.; Montgomery, J. A., Jr.; Vreven, T.; Kudin, K. N.; Burant, J. C.; Millam, J. M.; Iyengar, S. S.; Tomasi, J.; Barone, V.; Mennucci, B.; Cossi, M.; Scalmani, G.; Rega, N.; Petersson, G. A.; Nakatsuji, H.; Hada, M.; Ehara, M.; Toyota, K.; Fukuda, R.; Hasegawa, J.; Ishida, M.; Nakajima, T.; Honda, Y.; Kitao, O.; Nakai, H.; Klene, M.; Li, X.; Knox, J. E.; Hratchian, H. P.; Cross, J. B.; Bakken, V.; Adamo, C.; Jaramillo, J.; Gomperts, R.; Stratmann, R. E.; Yazyev, O.; Austin, A. J.; Cammi, R.; Pomelli, C.; Ochterski, J. W.; Ayala, P. Y.; Morokuma, K.; Voth, G. A.; Salvador, P.; Dannenberg, J. J.; Zakrzewski, V. G.; Dapprich, S.; Daniels, A. D.; Strain, M. C.; Farkas, O.; Malick, D. K.; Rabuck, A. D.; Raghavachari, K.; Foresman, J. B.; Ortiz, J. V.; Cui, Q.; Baboul, A. G.; Clifford, S.; Cioslowski, J.; Stefanov, B. B.; Liu, G.; Liashenko, A.; Piskorz, P.; Komaromi, I.; Martin, R. L.; Fox, D. J.; Keith, T.; Al-Laham, M. A.; Peng, C. Y.; Nanayakkara, A.; Challacombe, M.; Gill, P. M. W.; Johnson, B.; Chen, W.; Wong, M. W.; Gonzalez, C.; Pople, J. A. *Gaussian 03*, revision C.02; Gaussian, Inc.: Wallingford, CT, 2004.
(69) Dunning, T. H. In *Methods of Electronic Structure Theory*; Schaefer, H. F., III, Ed.; Plenum Press: New York, 1977.
(70) Shiga, M. Ab Initio PIMD Code; 2008.
(71) Martyna, G. J.; Tuckerman, M. E.; Klein, M. L. *J. Chem. Phys.* **1992**, *97*, 2635.
(72) Tobias, D. J.; Martyna, G. J.; Klein, M. L. *J. Phys. Chem.* **1993**, *97*, 12959.
(73) Tuckerman, M. E.; Parrinello, M. *J. Chem. Phys.* **1994**, *101*, 1302.
(74) Lax, M. *J. Chem. Phys.* **1952**, *20*, 1752.
(75) Ramírez, R.; López-Ciudad, T.; Kumar, P.; Marx, D. *J. Chem. Phys.* **2004**, *121*, 3973.
(76) Shiga, M.; Nakayama, A. *Chem. Phys. Lett.* **2008**, *451*, 175.
(77) Witt, A.; Ivanov, S. D.; Shiga, M.; Forbert, H.; Marx, D. Ruhr-Universität Bochum, Germany. Unpublished work, 2008.
(78) Moss, G. P. *Pure Appl. Chem.* **1996**, *68*, 2193.
(79) Seddon, W. A.; Fletcher, J. W.; Sopchyshyn, F. C. *Can. J. Chem.* **1976**, *54*, 2807.

JP8081936